Earth and Planetary Science Letters 420 (2015) 73–84

Contents lists available at ScienceDirect

Earth and Planetary Science Letters

www.elsevier.com/locate/epsl

Rapid and slow: Varying magma ascent rates as a mechanism for Vulcanian explosions

Mike Cassidy [a,*], Paul.D. Cole [a], Kelby E. Hicks [b], Nick R. Varley [c], Nial Peters [b], Allan H. Lerner [c]

[a] School of Geography, Earth and Environmental Sciences, Plymouth University, Plymouth, PL4 8AA, UK
[b] Department of Geography, University of Cambridge, Downing Place, Cambridge, CB2 3EN, UK
[c] Facultad de Ciencias, Universidad de Colima, Col., 28045, Mexico

ARTICLE INFO

Article history:
Received 18 July 2014
Received in revised form 26 February 2015
Accepted 3 March 2015
Available online 3 April 2015
Editor: T. Elliott

This paper is dedicated to Kelby Hicks, our friend and colleague who sadly passed away in April 2013, whilst collecting data in the field for this project

Keywords:
Volcán de Colima
effusive–explosive
microlites
SO_2
conduit dynamics
degassing

ABSTRACT

Vulcanian explosions are one of the most common types of volcanic activity observed at silicic volcanoes. Magma ascent rates are often invoked as being the fundamental control on their explosivity, yet this factor is poorly constrained for low magnitude end-member Vulcanian explosions, which are particularly poorly understood, partly due to the rarity of ash samples and low gas fluxes. We describe ash generated by small Vulcanian explosions at Volcán de Colima in 2013, where we document for the first time marked differences in the vesicularity, crystal characteristics (volume fraction, size and shape) and glass compositions in juvenile material from discrete events. We interpret these variations as representing differing ascent styles and speeds of magma pulses within the conduit. Heterogeneous degassing during ascent leads to fast ascending, gas-rich magma pulses together with slow ascending gas-poor magma pulses within the same conduit. This inferred heterogeneity is complemented by SO_2 flux data, which show transient episodes of both open and closed system degassing, indicating efficient shallow fracture sealing mechanisms, which allows for gas overpressure to generate small Vulcanian explosions.

1. Introduction

Vulcanian explosions are a typical expression of volcanism observed at intermediate to silicic volcanoes, yet the mechanism which controls the magnitude of such eruptions remains enigmatic (Morrissey and Mastin, 2000). These discreet, relatively small explosions are short-lived, lasting for only a few minutes and range in magnitude generating ash-rich plumes from small and frequent <1 km high ash-poor plumes as observed at Santiaguito (Guatemala), Semeru (Indonesia) and Volcán de Colima (Mexico), to >10 km high, as at Sakurajima (Japan) and the Soufriere Hills volcano (Montserrat) (Self et al., 1979; Morrissey and Mastin, 2000; Cole et al., 2002). These differ from another type of eruptive activity, Strombolian explosions, which are characterised by small, frequent (often several per hour) explosions that have been attributed to the rise of and bursting of large individual gas bubbles (Vergniolle and Jaupart, 1986). Large magnitude Vulcanian explosions are often accompanied by large SO_2 gas fluxes (>30 kg/s; Edmonds and Herd, 2007) and gas-rich magma, represented as pumiceous products (e.g. Cole et al., 2002; 2014; Clarke et al., 2007; Williamson et al., 2010; Wright et al., 2012; Miwa et al., 2013); whereas pumiceous or vesicular material is lacking in some Vulcanian explosions, attributed to a gas-dominated upper conduit as opposed to a conduit filled with vesiculated magma (Morrissey and Mastin, 2000). Magma ascent rate, the relative permeabilities of the magma and the walls of the conduit are thought to be the main factors controlling open-system gas release prior/during an eruption (Cashman, 2004; Gonnermann and Manga, 2007; Kennedy et al., 2010; Wright et al., 2012). More explosive Vulcanian eruptions have magma ascent rates an order of magnitude higher than effusive eruptions (effusive $\leq 10^{-2}$ m/s; explosive $\geq 10^{-1}$ m/s) and thus ascent rates are deemed to play a significant role in Vulcanian eruptions (Miwa et al., 2009). Shallow-level (<2 km) degassing, crystallisation and ascent rate conditions are key parameters in determining the conditions and processes that control Vulcanian explosions, therefore coupled high-temporal

* Corresponding author.
E-mail address: mcassidy@uni-mainz.de (M. Cassidy).

http://dx.doi.org/10.1016/j.epsl.2015.03.025

resolution SO_2 flux and quantitative petrographic measurements provide a key insight into these processes. Here, we present a combination of gas monitoring data with petrographic and geochemical analysis of ash collected from the explosions of Volcán de Colima in 2013, to shed light on the degassing and eruptive processes occurring. In particular this study, aims to constrain how magma ascent rates influence Vulcanian explosion dynamics, something that is not achievable with current geophysical techniques.

2. Background

Volcán de Colima, Mexico, is the most active volcano in North America and commonly displays Vulcanian explosions, often with accompanying lava flow or dome activity. Activity has continued intermittently since 1998, with six episodes of dome growth, each associated with periods of explosive eruptions (Zobin et al., 2002; Varley et al., 2010a). More commonly the effusive periods have been followed by larger magnitude Vulcanian explosions, but in the case of the 2005 episode effusion occurred simultaneously with some large explosions, producing pyroclastic density currents reaching up to 5.4 km from the volcano (Varley et al., 2010a). Since 2003, the volcano has also produced smaller Vulcanian-style events with repose periods in the order of hours, superimposed on top of the occasional effusion/larger Vulcanian explosive activity. In January 2013, Volcán de Colima resumed activity after 18 months of quiescence with three larger magnitude Vulcanian explosions subsequently followed by dome extrusion. Since then activity has continued in the form of lava dome emplacement, the development of a lava flow and small, but frequent Vulcanian explosions (10–30 per day from March to August 2013; Fig. 1B–D). These explosions commonly comprised multiple pulses and range from ash-rich plumes (Fig. 1D), grey in colour with exit velocities around 10 m/s although sometimes higher (measured by SO_2 camera imagery) with accompanying small ballistics, to ash-poor, white coloured plumes (Fig. 1B and C), less impulsive and slower exit velocities, hence smaller plume heights. Some explosions viewed at night showed abundant incandescent material that was ejected from the vent, indicative of the involvement of juvenile magma. In addition, flights over the crater following explosions, showed that they generally do not generate craters, thus indicating that the explosions do not incorporate much accidental material from around the summit (Fig. 1B). Most material therefore was derived from hot, recently (hours ago) ascended magma. Incandescent rockfalls from the dome and the lava flow were common and occurred both before and after explosions. Explosions originated from variable parts of the dome, often exploding from different points simultaneously, indicative of explosions erupting through a semi-permeable dome (Fig. 1). There is likely one vent beneath the dome but multiple gas pathways with sealing occurring, thus creating different points of origin of the explosions. These explosion locations were typically sporadic and unaffected by the magnitude of individual explosions.

3. Methods

Our multi-disciplinary approach to volcano monitoring, involves the measurement of SO_2 fluxes from the summit, as well as the collection of ash from the small Vulcanian explosions for subsequent quantitative crystal and micro-geochemical analysis.

3.1. SO_2 measurement

SO_2 fluxes were measured both by an SO_2 camera; giving high temporal and spatial resolution, but suffering from interference from ash and other gases (Dalton et al., 2009; Kantzas et al., 2010); and a UV spectrometer using the Differential Optical Absorption Spectroscopy (DOAS) method; where one SO_2 flux measurement takes ~40 s, but is generally more accurate than the SO_2 camera (Platt, 1994; Galle et al., 2003).

3.1.1. SO_2 camera data

An SO_2 camera (also known as a UV camera) (EnviCAM1) was used to record images at both 310 nm and 328 nm (using filters with a 10 nm bandwidth) from a distance of <3 km from Volcán de Colima. Clear weather periods, where clouds were not obscuring the volcano were chosen for the SO_2 measurements, and other spectral interferences were reduced by avoiding times where ash from rockfalls was drifting into the camera's field of view. Recommendations by Dalton et al. (2009) for ideal exposure times, background images and calibrations were followed to produce ~0.5 Hz image data. Four calibration cells were used to convert raw images to SO_2 concentration path length. A Matlab code (courtesy of Patricia Nadeau) was used to create profiles of the plumes, which were then integrated and multiplied by the calculated plume speed, following the method of Nadeau et al. (2011), to produce fluxes.

3.1.2. DOAS

UV spectra were collected using an OceanOptics USB2000 spectrometer coupled to a telescope with an optical fibre. The telescope was mounted on a small USB-powered scanning stage to enable acquisition across a full transect of the plume. Spectra were collected continuously during scanning, and scan-angles were computed in post-processing by comparing the creation times of the spectra files with an angle-versus-time file produced by the control software for the scanning stage. SO_2 column amounts were retrieved from the spectra with standard DOAS methodology (Platt and Stutz, 2008) using the DOASIS software (Kraus, 2006) and scripts written by Tsanev (http://www.geog.cam.ac.uk/research/projects/doasretrieval). Due to a lack of available calibration spectra, the width of the instrument function (assumed to be Gaussian) was estimated by fitting solar, ring and O_3 reference spectra to clear-sky data from the spectrometer. The full-width-half-maximum of the instrument function was left as a free parameter during the fitting and was found to have an optimal value of 0.6 nm. Processed spectra were split into individual scans and each scan was divided into in-plume and out-of-plume regions. A linear fit through the out-of-plume regions was used as an estimate of the background and subtracted from the scan. Integrated SO_2 column amounts were calculated using the standard scanning DOAS integration method (e.g. Salerno et al., 2009) and then converted to fluxes by multiplying by the plume transport speed, which was calculated using the SO_2 camera imagery.

3.2. Ash analysis

Ash generated by the frequent Vulcanian explosions at Colima was periodically collected at distances of between 0.6 and 6 km around the volcano (Fig. 1). All the tephra collected was <2 mm and thus ash grade. Cumulative samples representing ash from numerous explosions were collected by high-sided cylindrical collection vessels to minimise contamination. Sampling these products in the dry season ensured that all samples were not wet upon collection. In addition ash was sampled directly from fallout during 6 discrete, individual explosions at similar distances from the volcano.. In total, 13 of the cleanest and most voluminous samples from the 2013 activity were examined in further detail (Fig. 2). Two samples from the 2005 activity were collected from large explosions in a similar manner to the 2013 samples from Colima city and El Playon (Supplementary material A). These were also processed using the same methods as a comparison for the 2013 activity. A rockfall and a non-juvenile ballistic sample were also

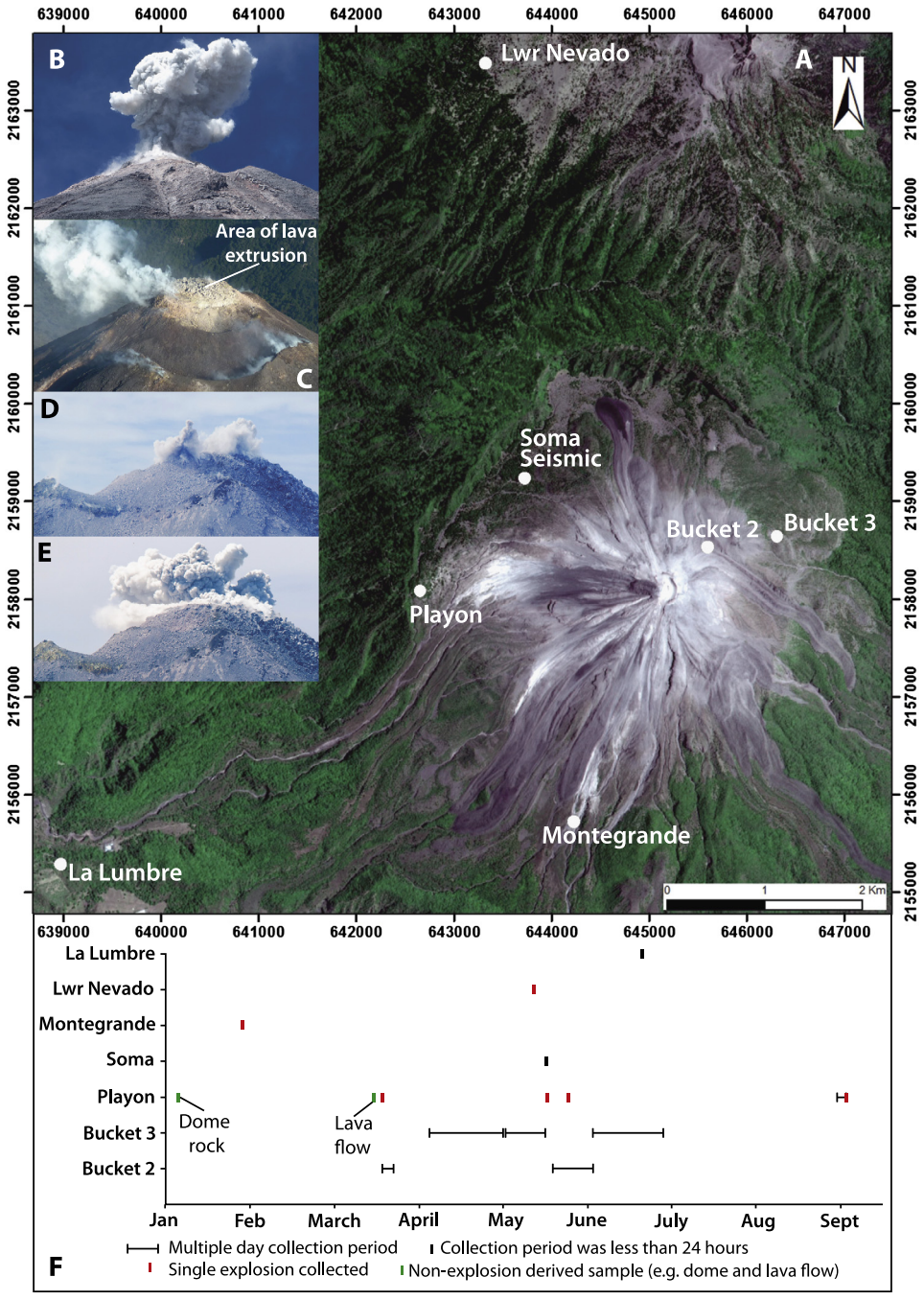

Fig. 1. A) True colour SPOT image taken on 05/05/13, showing the 7 sampling locations around Volcán de Colima. The co-ordinates are in UTM zone 13 N. B) This photo shows a typical Vulcanian explosion sampled in the study (taken on 24/03/13 from Montegrande), looking north. C) Oblique aerial photo taken from the south during an overflight on 20/06/13, looking north west. The photo was taken shortly after a small ash-poor explosion and shows the actively extruding dome. D) and E) Photos taken from Lwr Nevado at the onset of small Vulcanian explosions looking south, showing explosions were sourced from multiple locations on the dome (taken on 13/05/13 and 21/05/13 respectively). F) The sampling chronology and collection period for the samples used in this study. (For interpretation of the colours in this figure, the reader is referred to the web version of this article.)

examined for crystal analysis, representing material from the extruding lava flow and dome, or sub-dome region respectively. The ash was cleaned over a 63 micron sieve with deionised water and rinsed in an ultrasonic bath. Componentry (quantifying the abundance of different clast types), was carried out using a binocular microscope counting at least 300 grains to be statistically representative.

Grain size analysis was conducted by laser diffraction on a Malvern Mastersizer 2000, which is able to measure 0.02 to 2000 µm grain sizes. The particles are kept in suspension by in-built stirrers and the sample is pumped continuously through the Malvern analyser to ensure random orientation of the particles relative to the laser beam. Light obscuration was between 10 and 20%. Standard materials with mean diameters of 32 and 125 µm were used to monitor accuracy, while 5 repeat runs for each sample were used to monitor precision (reported at $<0.5\%$ SD) (Supplementary Table B).

3.3. SEM and electron microprobe analysis

The juvenile components (Section 4.1) from the ash were picked, set in resin, polished and carbon coated in preparation for

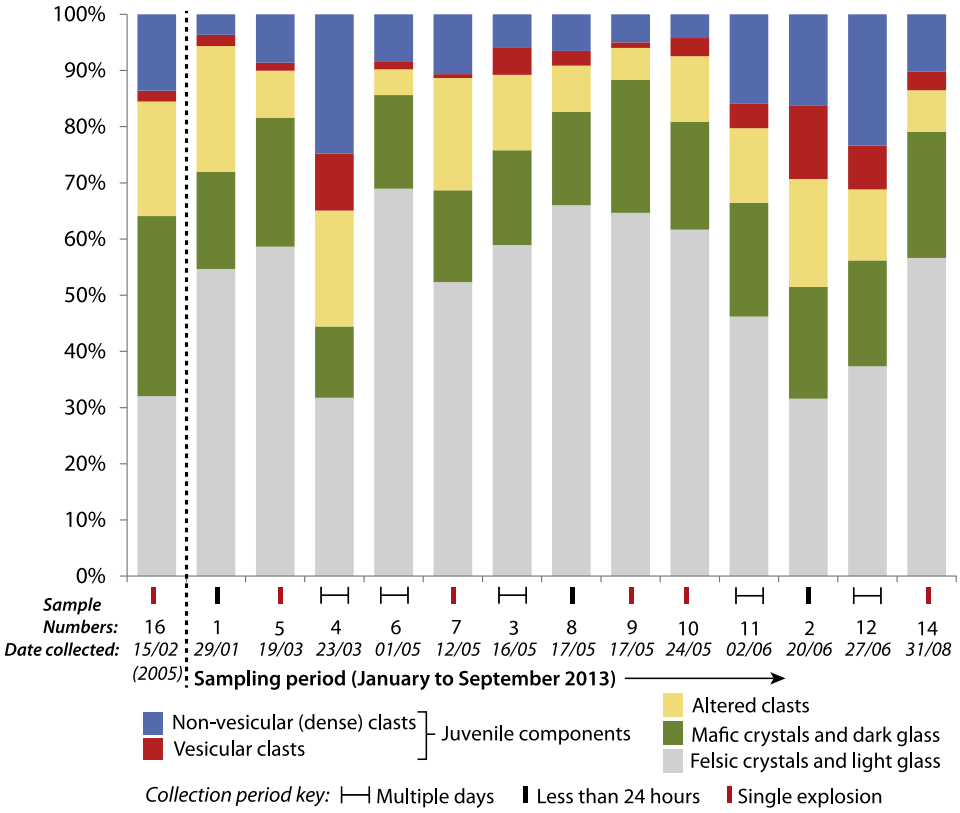

Fig. 2. Componentry of the ash fallout samples collected from Vulcanian explosions, which are explored in this study, based on the 63–125 μm size range. The samples are plotted in chronological order, a representative sample from 2005 is added for comparison.

electron microprobe and SEM analysis. Thin sections of the ballistic and lava flow samples were made at the geology department at the University of Durham.

SEM analysis was conducted using a JEOL 6610 LVSEM at the Plymouth University micro-analysis unit. Carbon-coated samples were imaged at 15 kV, a working distance of 10 mm, a spot size of 40–50 μm and a nominal probe current of 50–500 pA, using both secondary electron (SE) and backscattered electron (BSE) detectors. Quantitative crystal textural analysis was conducted on backscattered SEM images, the magnification varied depending upon the microlite size and density. Feldspar microlite crystals were outlined manually using Adobe Illustrator, at least ~400 crystals were measured in each sample, over an area generally ranging from 10,000 to 30,000 mm^{-2}. These digitised images were then converted to high-resolution TIFF files, so that crystal measurements could be made using ImageJ (version 1.48). Mean crystal area, crystal volume fraction, and crystal dimensions (short and long axes) were measured, the latter using a best-fit ellipsoid method. Microlite number density was calculated by dividing the number of whole crystals in the analysed area by the area of groundmass (mm^{-2}). The results of these data can be found in Supplementary Table C.

The major element compositions of the glasses, microlites and phenocrysts were determined using the Cameca SX100 electron microprobe at the University of Bristol. Quantitative determinations of elements were made using the wavelength dispersive system with TAP, PET and LIF crystals. A range of metal, oxide and silicate (e.g. jadeite, wollastonite) standards were used for calibration of the spectrometers. All analyses used an accelerating voltage of 15 kV. For pyroxene and plagioclase a spot size of 4 μm and a 100 nA beam current was used. Multiple points were targeted within the larger microlites (>30 μm), using a 4 μm spot size to ensure the analyses were reproducible (standard deviation <2% for all elements). The data were checked for totals (any data outside the 97–101% were discarded) and consistency with other points within the same microlite. For glasses, a 10 μm spot was used with a beam current of 60 nA for Cl, F, S, P, Cr and Ni, and 4 nA for all other elements, with counting times of 50–200 s per analysis. During glass measurements, Na peaks were counted first to avoid significant migration during the run. In addition to calibration of each X-ray line, a series of secondary reference standards (olivines, pyroxenes, feldspars and glasses) were measured daily to check accuracy, precision and totals. Accuracy was generally better than 5% for most elements, based on repeat analyses of EMPA secondary standard BCR2 (Columbia River Basaltic glass, courtesy of Smithsonian) and by comparison with reference concentrations for the standard, with the exception of TiO_2, K_2O and P_2O_5, which were better than 20–35 % (Supplementary material D).

4. Results and discussion

4.1. Ash components

The collected ash comprised juvenile material including both felsic and mafic crystals often with adhering glass (average 70% volume of clasts), and altered fragments (13%), poorly-vesicular (dense) glassy clasts (13%) and vesicular glassy clasts (4%) (Fig. 2). The cumulative ash samples representing numerous explosions are indistinguishable in terms of components, chemistry and petrography to those of single explosions and thus are considered comparable (Fig. 2). The mean grain sizes range from 5Φ (30 μm) to 2Φ (240 μm) and generally display uni-modal grain size distribution peaks. The dense and vesicular clasts were unaltered, glassy in appearance and thus were considered to be juvenile. The dense and vesicular clasts differ considerably in their appearance; not only the vesicularity but also crystallinity (Fig. 3). The dense clasts form between 3 and 25 vol% of the ash sample, are grey in colour, and range in vesicularity from 0 to 15% (Fig. 3C). They contain phenocrysts (>100 μm) of plagioclase, ortho- and clino-pyroxene and

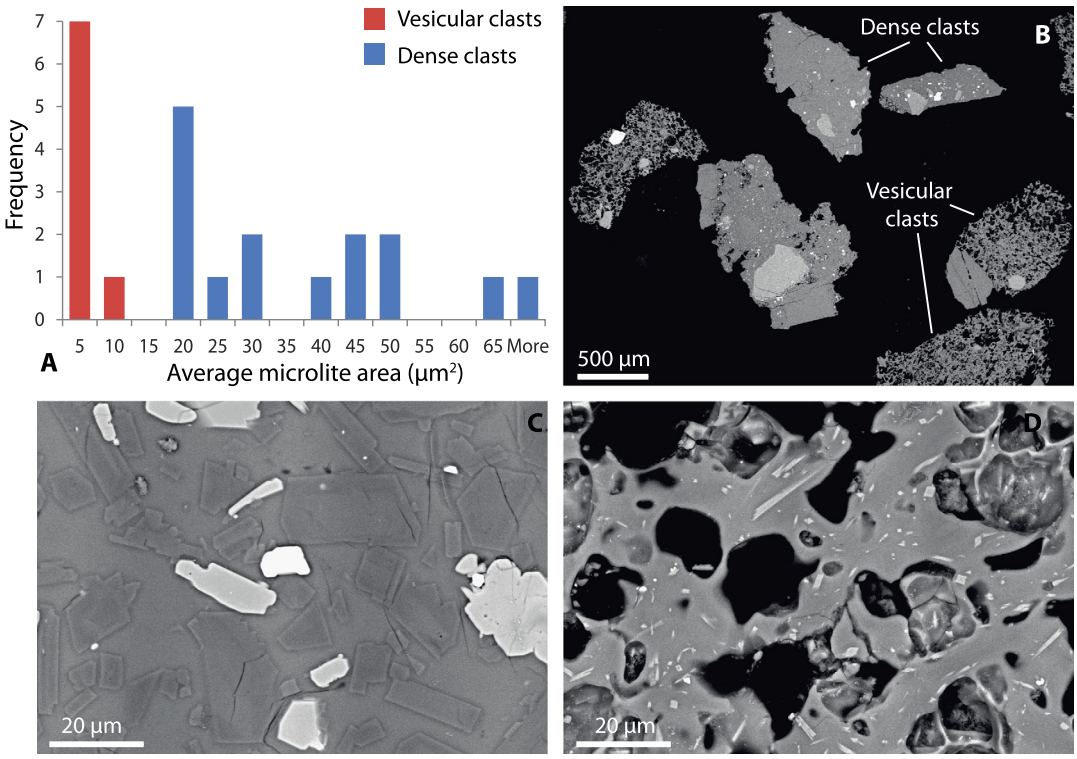

Fig. 3. A) Histogram showing the difference in microlite crystal sizes between the vesicular and dense clasts. B) Backscattered SEM image of both the vesicular and dense clasts referred to in this study. C) Backscattered SEM image of a dense clast showing large, prismatic microlites, comprised dominantly of feldspar and pyroxene. D) Backscattered SEM image of a vesicular clast, with lower crystallinity, and small, acicular microlites comprised of pyroxene and Fe-oxides.

titanomagnetite. The groundmass comprises microlites with an assemblage similar to the phenocryst phases and those present in the dense clasts are at large end-member microlite size (average 40 μm long; Couch et al., 2003a). The microlites were nominally equant to prismatic in shape (short/long axis ratio of 0.6) and average microlite number densities are 17,300 mm^{-2}. Microlite crystallinity ranges from 35 to 56%. Samples of the lava flow which had fallen downslope and ballistic samples ejected during the powerful Vulcanian explosions at the beginning of January were found to be very similar in character to these dense clasts (Supplementary Fig. S1).

Vesicular juvenile clasts form between 1 and 13% of the ash deposit, they are pale yellow coloured, ranging in vesicularity from 20 to 50%. They contain a similar assemblage of phenocrysts as the dense clasts, but the microlites comprise of Fe–Ti oxides and rare pyroxenes, little or no feldspar is found in the microlite component. Microlite sizes are notably smaller than for the dense clasts (average 3 μm; Fig. 3D) with their shape more commonly being acicular (short/long axis ratio of 0.5). Microlite number densities are 51,400 mm^{-2} on average and crystallinity ranges from 3 to 25% (Supplementary Table C).

4.2. Geochemical differences

Matrix glass compositions between the dense and vesicular juvenile components differ markedly. Dense clasts have SiO_2 contents ranging from 73 to 77 wt% and are generally more crystalline (average 46% vol microlites) whereas the vesicular clasts are less crystalline (average 15% vol microlites) and contain considerably lower glass SiO_2 contents (60–68 wt%) (Fig. 4A). Several lines of evidence suggest that these glassy clasts, although texturally and compositional different, were derived from the same magma source. First, all the analysed phenocryst feldspar cores have the same composition (Fig. 5). In addition, crystal profiles show that they comprise similar trace element contents and traverses across plagioclase grains showed little change in trace elements such as Fe, Mg or Ti with anorthite content, which would otherwise indicate melt disequilibrium by a different composition (Ruprecht and Worner, 2007) (Supplementary Fig. S2). Finally, there were no textural indications of magma mixing or mingling between the two magmas, such as enclaves, sieve textures or resorption, consistent with the notion that one magma may have evolved from the other. The anorthite content of the phenocryst rims differ slightly between the two different clasts types; plagioclase phenocryst rims of the vesicular clasts span from $An_{47–58}$, but the plagioclase phenocryst rims and microlites in the dense clasts occupy a larger range and generally lower An contents ($An_{18–56}$). No data were obtained for the plagioclase microlites in the vesicular clasts as the crystals were too small to analyse with the techniques available.

We interpret this compositional variation in glass chemistry between vesicular and dense clasts (Fig. 4) as being the result of fractional crystallisation, where variable decompression crystallisation has occurred to enrich the glass in SiO_2 (Hammer et al., 1999; Cashman and Blundy, 2000; Blundy and Cashman, 2001; Couch et al., 2003b; Blundy and Cashman, 2008). To test this we have successfully recreated the dense glass composition starting from a vesicular glass composition by crystallising 35% plagioclase, 6% pyroxene and 4% magnetite microlites using mass balance (to within 1 wt% for all major elements, excluding Na, which is still within 2 wt% of the glass average for the dense clasts; Supplementary Material E). The microlite proportions used for this calculation are similar to the average modal proportions measured in the dense clasts (Supplementary Material C). The wide range of microlite anorthite contents, coupled with the elevated SiO_2 contents in the dense clasts (>72% SiO_2; Fig. 4) strongly suggests that the dense clasts crystallised and differentiated at a shallow level (less than 100 MPa) by decompression and gas loss (Cashman and Blundy, 2000). By contrast, ash fallout samples from eruptive events in 2005 (a period which was particularly explosive; Varley et al., 2010a) contain little or no vesicular material (<4% vol;

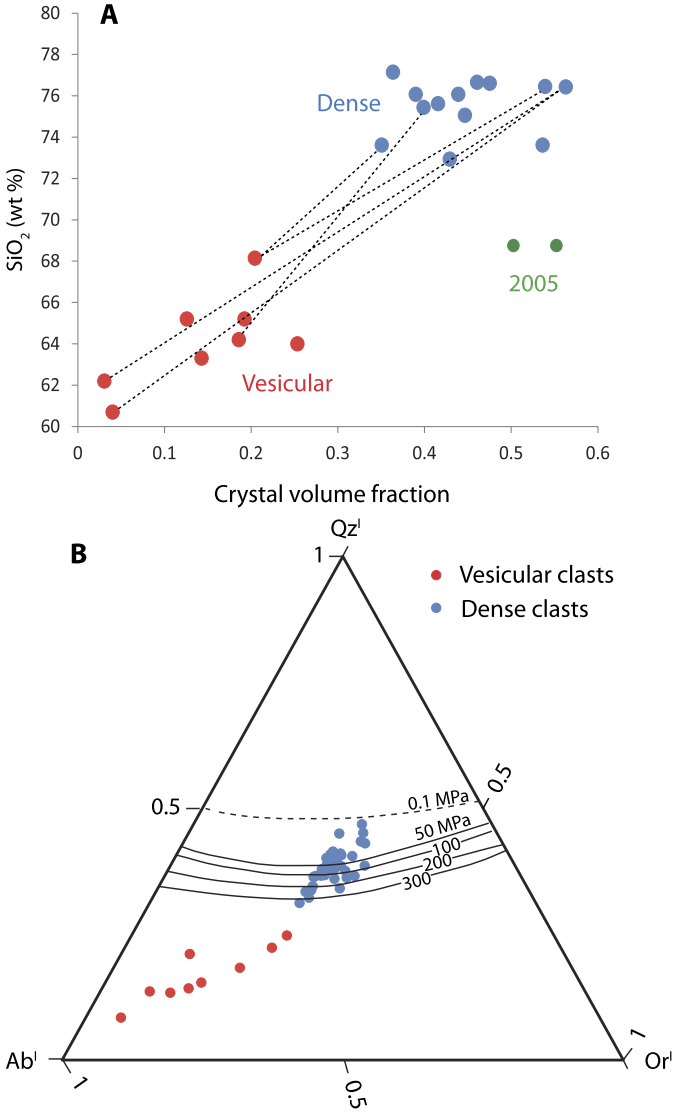

Fig. 4. A) Plot showing the variation of glass composition and crystallinity between the dense and vesicular clasts. Tie lines indicate the range observed in a single ash sample. B) Glass compositional data plotted on the haplogranite system (Blundy and Cashman, 2001) to show liquid lines of decent. The phases represent Ab – Albite, Qz – Quartz and Or – Orthoclase. (For interpretation of the references to colour in this figure, the reader is referred to the web version of this article.)

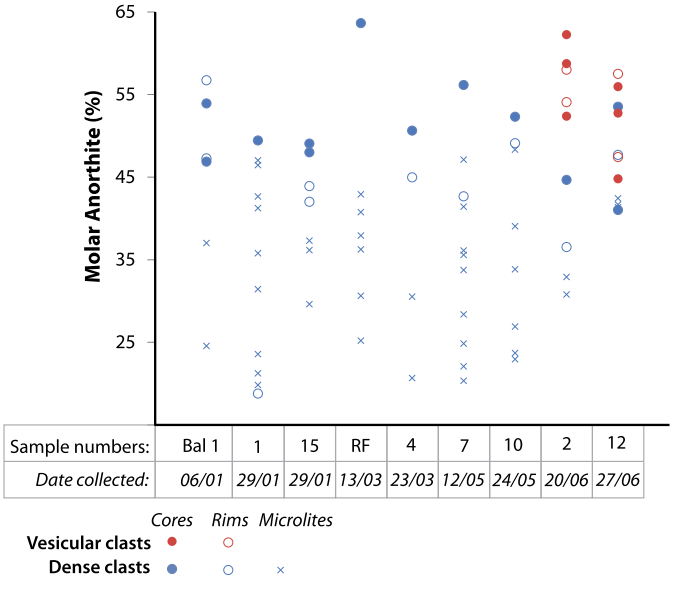

Fig. 5. Feldspar point data from phenocryst cores, rims and microlites measured for both the vesicular (red symbols) and dense (blue) clasts. This is plotted by samples in chronological order. Sample RF is a rockfall sample from the active lava flow. Bal 1 is a ballistic bomb representing dome or sub-dome material and sample 15 is from a pyroclastic density current deposit. The remainder of the samples used in this plot are ash fallout samples from Vulcanian explosions. Glass compositional data plotted on the haplogranite system (Blundy and Cashman, 2001) to show liquid lines of decent. (For interpretation of the references to colour in this figure legend, the reader is referred to the web version of this article.)

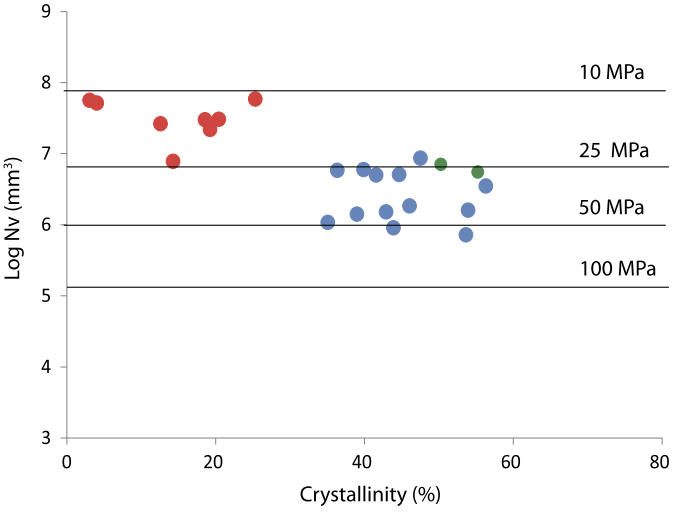

Fig. 6. Microlite number volume (Nv) against crystallinity (Blundy and Cashman, 2008) for the vesicular (red), dense (blue) clasts and 2005 samples (green). This shows approximate microlite formation depths (shown in Fig. 8). (For interpretation of the references to colour in this figure legend, the reader is referred to the web version of this article.)

Fig. 2). The data suggest that larger quantities of dense, gas poor magma were incorporated in these larger explosions effectively diluting the gas-rich magma.

Magmatic temperatures and approximate water contents for the 2013 erupted material from Volcán de Colima were estimated from the experimentally calibrated plagioclase-melt geothermometer and hygrometer of Putirka (2008). These estimates show that the vesicular magma was hotter and wetter than the dense magma (~1030–1100 °C and ~1.7% H_2O), whereas the dense magma was distinctly cooler and more degassed (~830–890 °C and ~1% H_2O), consistent with estimates from Reubi et al. (2013) and Savov et al. (2008). In these studies measured water contents were <4% from pyroxene-hosted melt inclusions and estimated temperatures ranged from 980 to 1030 °C for the 2005 magmas.

4.3. Ascent styles and rates

Plagioclase microlite compositions in the dense clasts record a wide range of anorthite contents, suggesting that these microlites formed at a range of different temperatures, pressures and water-contents indicating multi-step decompression (Fig. 5). Shallow decompression crystallisation of the dense clasts is further supported by the plot of glass compositions on the haplogranite system (Blundy and Cashman, 2001) (Fig. 4B). Liquid lines of descent of the glass from the dense clasts show that the glass composition has gradually evolved over a wide range of depths, from ~11 km (300 MPa) to the surface. In contrast, the vesicular clasts show limited evolution of the glass composition (i.e. minimal crystallisation) at shallow levels, indicating rapid ascent through the shallow system (Couch et al., 2003a). This is supported by estimations of microlite formation depths from microlite number

Table 1
A comparison of SO_2 fluxes and magma ascent rates for volcanoes which display similar Vulcanian activity.

	SO_2 tonnes per day (daily average)	Reference	Ascent rate (m/s)	Method and reference
Soufriere Hills (effusive)	500	Edmonds et al., 2003	1×10^{-3}–2×10^{-2}	Amphibole rims; Rutherford and Devine, 2003
Unzen (effusive)	180	Hirabayashi et al., 1995	2×10^{-3}–4.6×10^{-2}	Magnetite zonation; Venezecky and Rutherford, 1999; MND water exsolution rate meter; Noguchi et al., 2008
Mt St Helens (effusive)	610 (1980)–7 (1988)	Gerlach and McGee, 1994	2×10^{-3}–1.5×10^{-2}	Amphibole rims; Rutherford and Hill, 1993
Santiaguito (mild explosive/effusive)	70	Holland et al., 2011	7×10^{-3}–2.3×10^{-2}	Amphibole rims; Scott et al., 2012
Sakurajima (explosive)	1640	Mori et al., 2013	1.1×10^{-1}–3.5×10^{-1}	MND water exsolution rate meter; Miwa et al., 2009
Colima (effusive/explosive)	~1	This study	1×10^{-4} dense magma; 6.8×10^{-2} vesicular magma	MND water exsolution rate meter; this study

volumes (Fig. 6). These suggest that microlites within the dense magmas started forming at deeper depths, whereas microlites that are present in the vesicular magma formed nearer to the surface (Fig. 6). These small microlites, which formed just before or during an eruption, did not differentiate the glass composition enough to alter the haplogranite liquid line of decent, as evidenced in Fig. 4. However these must be considered gross estimates as the Colima rocks have not been subjected to decompression experiments required to calibrate them (Blundy and Cashman, 2008).

In order to test the hypothesis whether limited crystallisation of the vesicular clasts can be attributed to the fast rise of these magmas, ascent rates were estimated for the two different clast types using the water exsolution model of Toramaru et al. (2008). Equations for decompression rate (dP_w/dz; Eq. (1)) and ascent rate (V_n; Eq. (2)) were used to determine the cause for the two different crystallisation histories. These equations are summarised below, but further details about this method can be found in Toramaru et al. (2008).

$$\left|\frac{dP_w}{dt}\right| = \frac{c}{b}\left(\frac{N}{a}\right)^{\frac{2}{3}} \tag{1}$$

Here $c =$ is a function of water content, $b =$ constant, 40 for plagioclase and 17 for clinopyroxene, $a =$ calculation based on glass composition and water content and $N =$ microlite number volume. Water contents of 1.7% and 1% were used for the vesicular and dense clasts respectively (estimated using plagioclase-melt hygrometry), however microlite number volumes and glass composition data are the most sensitive factors affecting decompression rate. From this the ascent rate can be calculated:

$$V_n = \frac{1}{\rho g}\left|\frac{dP}{dz}\right|_{z=zn} \tag{2}$$

Here $\rho =$ density, $g =$ gravity, $dP_w/dz =$ decompression rate at a given water-content based on depth (z).

To compare the water exsolution rate meter (Toramaru et al., 2008) with other methods used to derive magma ascent rate, ascent rates were calculated for ash fallout samples collected from the 2005 explosive activity and compared with the estimates from Reubi et al. (2013), which are based on H_2O diffusive re-equilibration of melt inclusions for the 2005 ballistic ejecta samples. Toramaru et al. (2008) calculation used in this study yielded ascent rates of 7×10^{-4} m/s for a the 2005 ash fallout samples (based on glass compositions from Savov et al., 2008 and a water content of 1% from Reubi et al., 2013), which is directly comparable with Reubi et al. (2013) ascent rate estimate of 5×10^{-4} m/s. Significantly, ascent rates estimated using the Toramaru et al. (2008) method provided different magma velocities for the two different 2013 clasts observed in this study; an estimate of 1×10^{-4} m/s for the dense magma and 6.8×10^{-2} m/s for vesicular magma. The dense magma ascent rate is the same order of magnitude, but slower than the 2005 Volcán de Colima activity (7×10^{-4} m/s) and an order of magnitude slower than the effusive/dome building episodes from the Soufriere Hills, Mt St Helens, Unzen and Santiaguito (see Table 1 for comparison values). In contrast, the vesicular magma ascent rate estimate sits between the higher dome-effusion rates for the aforementioned Soufriere Hills, Mt St Helens and Unzen volcanoes and the higher ascent rates calculated in powerful Vulcanian explosions from Sakurajima (Table 1), and is two to four orders of magnitude slower than those (inferred from dehydration rates) of Sub-Plinian eruptions (Izu-Ohshima 1986 eruption; Toramaru et al., 2008). Unsurprisingly, this indicates that the ascent rate of magma plays an important role in the style of volcanic eruptions (Miwa et al., 2009; Miwa and Geshi, 2012; Wright et al., 2012) but in particular, this study shows how different magma ascent rates and styles may be causing rapid shifts from explosive to effusive activity.

4.4. Degassing processes

The high viscosity of silicic magmas inhibits the release of volatiles, thus increasing the possibility that gas escape will occur explosively (Mangan et al., 2004; Scandone et al., 2007). However if volatiles stored within the magma are lost during ascent this will lead to the passive extrusion of lava dome or flow (Eichelberger et al., 1986; Cashman, 2004). Volcán de Colima is classed as an open-vent volcano (Rose et al., 2013) and shows frequent transitions between open and closed degassing behaviour. SO_2 flux time series data (Fig. 7) provide an insight into the role of degassing in these small Vulcanian explosions. During the periods between explosions degassing appears to be closed-system, with very little or no SO_2 being released (Fig. 7). However, an almost instantaneous elevation in SO_2 flux occurs at the onset of an explosion, shown by both the SO_2 camera and the DOAS data, indicating short-lived open-system behaviour as the gas levels decrease gradually back to background values over 2–11 min (Fig. 7). Interestingly, longer periods were observed for the vent sealing process during the 2003–2011 activity (1–2 h; Varley et al., 2010b). The degassing episode exceeds the timescale of the explosions (average 7 min; Figs. 7A and B), if one assumes that the seismic signal represents the duration of the explosion. This is reflected in the shape of the SO_2 flux peaks, with large initial peaks resulting from gas released by the explosion and the sustained trailing tail from subsequent open-system degassing. This was also observed during the periods of explosive activity during the 2003–2011 active period (Stevenson and Varley, 2008). The high-temporal resolution of the SO_2 camera data show multiple peaks in the SO_2 flux time series during the explosions (Fig. 7). In some cases, where a series of explosions occur in quick succession, the system reverts back to low or almost no SO_2 flux before the next explosion occurs (Fig. 7B). This indicates that an efficient sealing of the conduit is occurring. When the total SO_2 masses released in each explosion are plotted against the repose

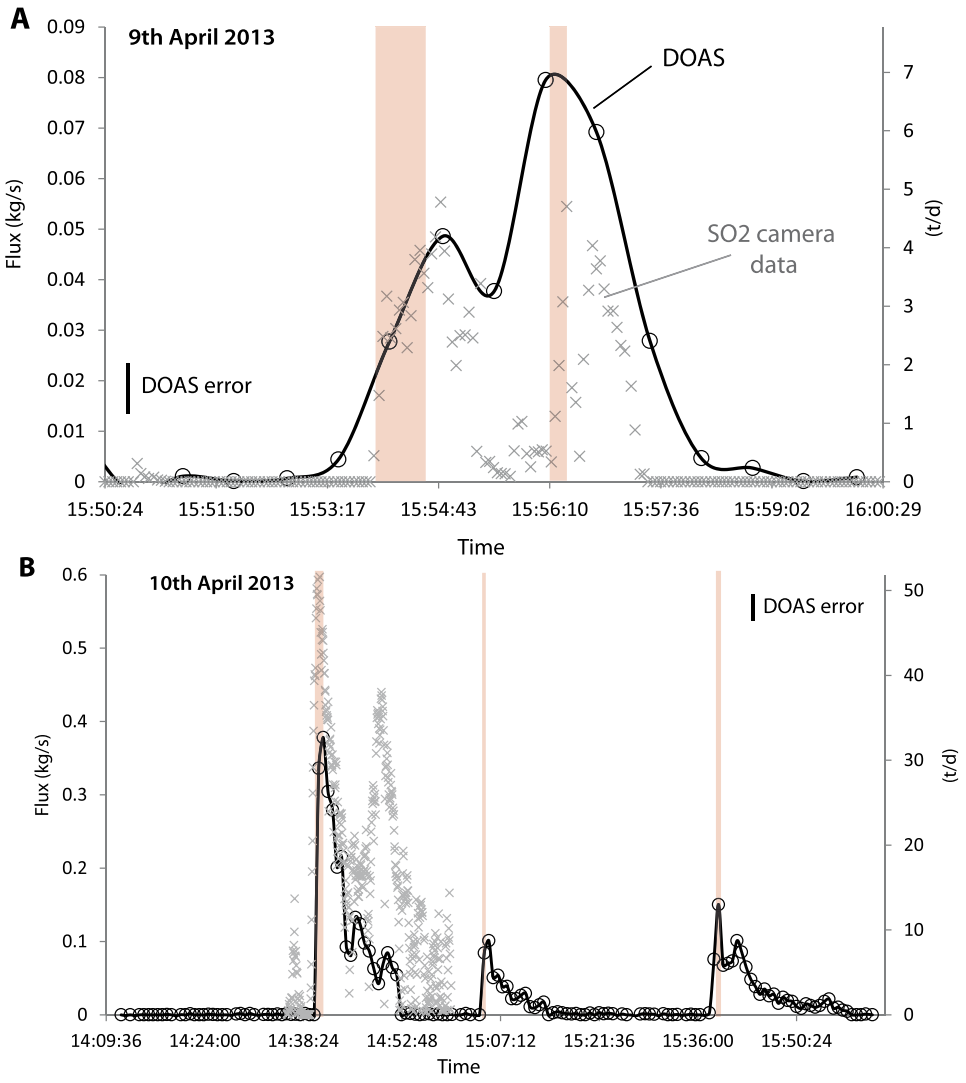

Fig. 7. A) and B) Degassing SO_2 flux time series profiles of explosions measured with an SO_2 camera and DOAS techniques. Red zones indicate the length of explosions according to seismometers. (For interpretation of the references to colour in this figure legend, the reader is referred to the web version of this article.)

time before the eruption, there is weak but apparent positive relationship (Fig. 8). This correlation implies that gas overpressure provides the force initially required to exceed the confining pressure and explosively fracture magma in the upper conduit to generate a Vulcanian explosion. This process of gas impedance by conduit sealing has been observed or inferred at other silicic volcanoes cf. Ngauruhoe (Self et al., 1979), Karymsky (Fischer et al., 2002), Tarawera (Kennedy et al., 2010), Sakurajima (Yokoo et al., 2013), with a similar model proposed for Volcán de Colima (Varley et al., 2010b).

By integrating the amount of SO_2 flux of all explosions for which there are data and calculating assuming an average SO_2 quantity per explosion (~58 kg; Fig. 8) we estimate SO_2 emissions of ~900 kg per day (0.9 tonnes per day). The small volumes of volatile-depleted magma (Savov et al., 2008; Reubi et al., 2013) coupled with the very low levels of continuous passive degassing during periods of repose potentially accounts for the anomalously low SO_2 daily output compared to other andesitic dome-forming volcanoes (Table 1).

The low gas fluxes measured at the summit coupled with the low volatile contents measured from the rocks erupted during the recent dome cycles at Colima (Savov et al., 2008; Reubi et al., 2013), suggest that a significant amount of volatiles are lost from the magma prior to eruption. Significantly, the contin-

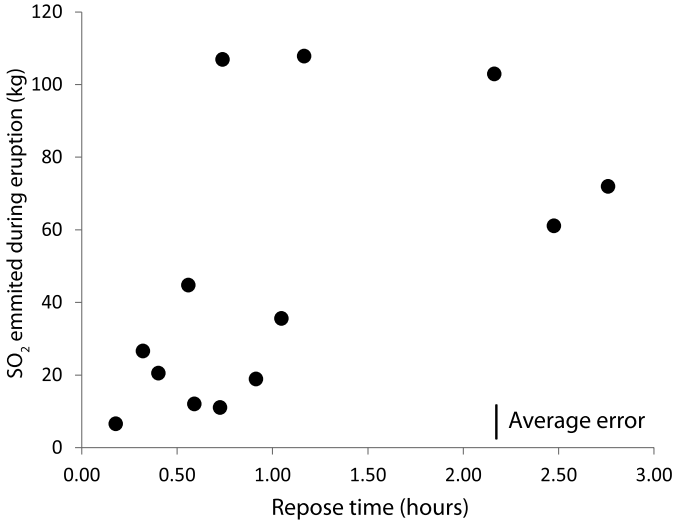

Fig. 8. Integrated SO_2 amounts from explosions plotted against the repose time before an explosion.

uous flux of SO_2 progressively decreased from the onset of the 1998–2011 eruption, with the trend continuing in 2013–2014. Moore and Carmichael (1998) and Carmichael (2002) suggested that Volcán de Colima andesitic magmas are generated from degassing and re-equilibration during ascent of hydrous parental magmas containing initially at least 6 wt% H_2O. According to Reubi et al. (2013) the relatively low maximal H_2O contents in Colima 1998–2005 magmas are a consequence of their relatively high temperatures leading to degassing before the onset of vapour-saturated crystallisation (Reubi et al., 2013). This extensive degassing process causes heterogeneity within the magma, which is preserved in the range of volatile contents recorded in the eruptive products (Reubi et al., 2013). We consider that it is this heterogeneity which may lead to different original ascent rates (accentuated by further, late-stage degassing) and therefore generating the gas-rich and gas-poor magma batches described here.

4.5. Conceptual model

In light of the results explored in this study, we present the following model to explain the degassing patterns and the variations in clast componentry, crystal characteristics and glass geochemistry found within recent ash fallout deposits from Vulcanian explosions at Volcán de Colima. We suggest that during the 2013 activity, the multiple vents previously observed (Lavallee et al., 2012) have not been active on the basis that explosions and lava effusion appear to be sourced from the same region (Fig. 1B, C and D). Initial activity in late January and February 2013 showed magma being extruded from a single source at the summit. In the case of explosions, they are sourced through a dome, with spatially and temporally variable permeability (Fig. 1B, C and D). We propose that the two different clast types observed in the explosion-derived ash are produced by magmas which originated from the same source, but were modified by differential degassing within conduit and/or shallow storage systems. We envisage that the system at Volcán de Colima comprises a magma-filled conduit, on the basis on the continued extrusion of magma at the surface. Therefore the two magma pulses with differing ascent rates must pass through each other, explaining the presence of the two different densities of magma within any one event, the mechanism by which this occurs is explored below and in Fig. 9.

The likely shallow level processes that govern activity at Volcán de Colima based on the findings from this study are illustrated in Fig. 9. During ascent, magma close to the conduit walls loses gas by lateral diffusion through the sides of the conduit (dense/gas-poor magma, coloured blue in Fig. 9), and begins to crystallise with microlites forming as deep as 3 km (Fig. 6). This crystallisation promotes differentiation of the remaining glass groundmass (Fig. 4). The increased crystallinity and elevated SiO_2 content makes the magma become more viscous, this coupled with the loss of volatiles reduces its buoyancy, which slows ascent of the magma. Small magnitude long-period seismicity is generated due to brittle deformation of the crystallising magma close to the conduit walls (Varley et al., 2010a). Ascent of the gas-poor magma is staggered (multi-step decompression; Figs. 4 and 6B) and likely collects in a shallow level storage system (~1 km) as indicated by melt inclusion data from Reubi et al. (2013) (Fig. 9).

In contrast, magma in the central part of the conduit experiences minimal gas loss making the magma more buoyant and thus rise more rapidly (vesicular/gas-rich magma, coloured red in Fig. 4B). The reduced ascent time results in less microlite crystallisation and glass differentiation (Fig. 4) and when coupled with higher temperatures, makes this vesicular magma less viscous then the dense magma. This allows pulses of gas-rich (vesicular) magma to ascend rapidly through the slowly ascending gas-poor (dense)

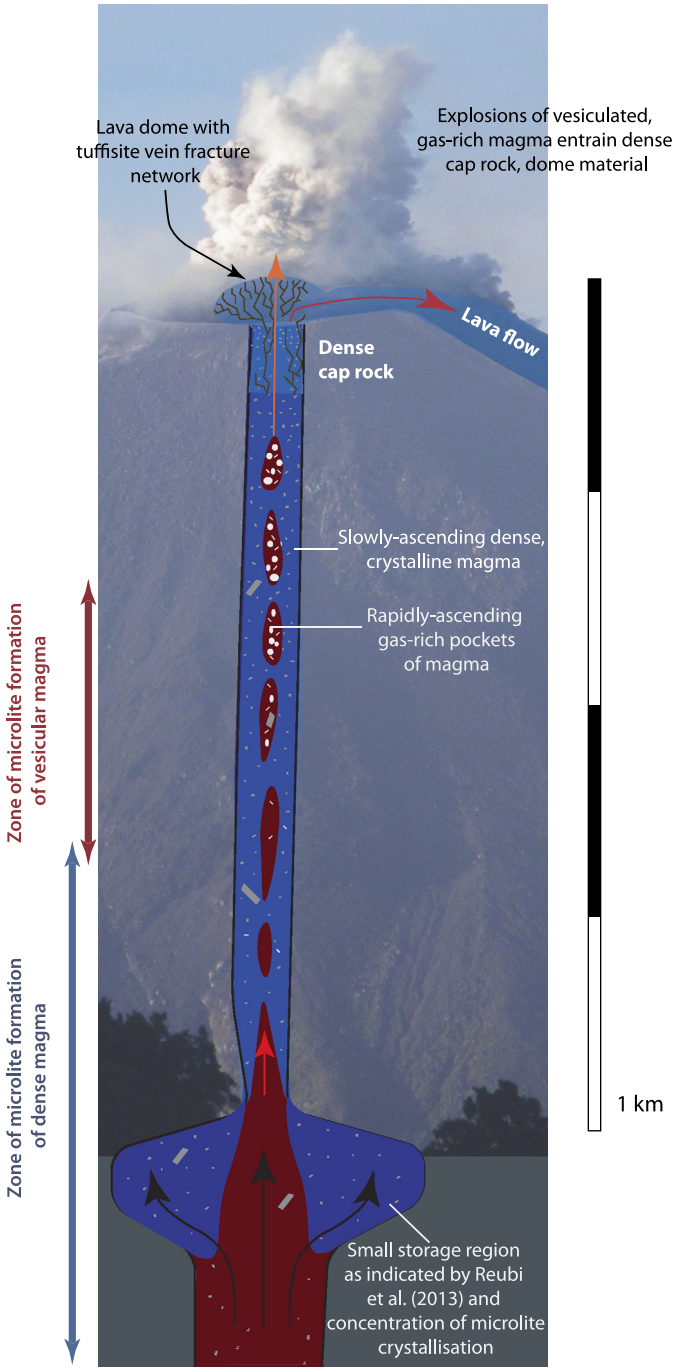

Fig. 9. Conceptual model of shallow processes occurring at Volcán de Colima. Blue portions represent the dense, slowly ascending magma and red, the vesicular, gas-rich and fast ascending magma. Explosions lead to open-system degassing and increased extrusion of dome and lava flows, degassing emissions are shut off as the conduit becomes sealed by the formation of tuffisite veins. The horizontal axis is slightly exaggerated, the crater is 250 m across for reference. (For interpretation of the references to colour in this figure legend, the reader is referred to the web version of this article.)

magma and transports dissolved gases from deep depths, providing the generation mechanism for the Vulcanian explosions. Indeed, separate inferences based on ^{210}Pb–^{222}Ra disequilibria of the 2005 andesite samples from Colima (Reubi et al., in press), also support the notion of discrete magma batches with variable degassing histories, variable ascent paths and rates, but the authors infer that this is likely due to multiple conduits within the 2005 system. Although this could be the case for the 2013 system, we

suggest this is unlikely based on our observation of a single explosion and extrusion source at the summit and the inference that the magma supply is coming from a single source at depth (Section 4.2).

4.6. Explosion mechanism

The impulsive nature of the explosions, reaching exit velocities of >10 m/s (consistent with previous Vulcanian explosions at Colima; Webb et al., 2014), coupled with the gradual cessation of SO_2 emissions over time (Fig. 7B) indicates low conduit and dome permeability prior to explosions. Variations in crystal and bubble concentrations along with volatile content heterogeneities promote piecemeal fragmentation of the magma as demonstrated in the pulsatory SO_2 flux time series (Fig. 7).

Fragmentation in these small magnitude Vulcanian explosions may be enhanced by the presence of more porous magma, which acts to lower the fragmentation threshold (Spieler et al., 2004) and increase the ejection velocity (Alatorre-Ibarguengoitia et al., 2011). Once the gas-overpressure is released by an explosion, both the vesicular and dense magma fragment and some accidental material from the dome/conduit walls may also be entrained. More energy is required to fragment the dense magma, so once all the gas-rich vesicular magma has erupted, the magma may cease to fragment further due to the higher fragmentation threshold of the dense magma (Spieler et al., 2004; Kennedy et al., 2005; Alatorre-Ibarguengoitia et al., 2011). This allows for open-system degassing, leading to effusive activity, where magma can degas freely and be extruded as a lava flow/or dome, and is supported by digital image correlation data from infrared time lapse imagery showing dome growth following explosions (Fig. 5; Walter et al., 2013). The vesicular magma pockets which are not erupted may then degas, forming crystals and then assimilate with the dense magma. The extrusion of degassed magma and fluxing of gas and pyroclastic material through the dome fractures acts to seal the conduit, limiting degassing and thereby allowing gas to accumulate prior to the explosions (Fig. 8).

5. Conclusions and implications

Recent models for Vulcanian explosions have considered vertical differentiation of batches of gas-rich and gas-poor magma, whereby vesicularity increases with depth and the gas-poor and gas-rich batches ascend at the same rate within the conduit (Wright et al., 2007; Clarke et al., 2007; Burgisser et al., 2010; Michaut et al., 2013; Miwa et al., 2013). Horizontal gradients have also been suggested, as cooling, degassing and crystallinity are expected to be highest at the conduit walls (Sparks et al., 1999; Tuffen et al., 2003; Kennedy et al., 2005; Edmonds and Herd, 2007; Varley et al., 2010a). Lane et al. (2008) and Burgisser et al. (2010) suggest that these two views may not necessarily be opposed, instead they invoke a heterogeneous transition zone composed of an intimate mingling between vesicular and dense magma, causing piecemeal-like fragmentation, whereas a much more homogeneous column below could have fragmented at once. In this study we show that Vulcanian explosions may be controlled by the different ascent style and rates of gas-rich and gas-poor magma pulses. This model proposes for the first time that gas-rich magma batches ascend through denser magma batches, which are located along the conduit walls. We suggest this is possible despite the moderate viscosities of both magmas as there is a large viscosity difference between them, attributed to their differences in crystallinity, melt composition, temperature and volatile contents. This mechanism is not unlike models proposed at basaltic Strombolian eruptions (Lautze and Houghton, 2007; Andronico et al., 2009) and therefore indicating that similar processes appear to occurring in both Vulcanian and Strombolian eruptions. The gas-rich batches observed in other Vulcanian explosions, may too have different ascent styles and rates, as observed in Table 1 and thus could exert an important control on the style and magnitude of Vulcanian eruptions.

Acknowledgements

We wish to thank Patricia Nadeau for her Matlab code, Arjan Dijkstra, Jodie Fisher, Glenn Harper and Richard Hartley at Plymouth University for lab assistance. Jonathan Barry, Steffano Vissani and other CIIV volunteers for field assistance. Kayla Iacovino and Yves Moussallam at the University of Cambridge for development of the DOAS code. Stuart Kearns for assistance with EPMA analysis at the University of Bristol. Discussions with Katie Preece, Arjan Dijkstra, Tamsin Mather and David Pyle helped to progress the ideas in this manuscript. The constructive comments of two anonymous reviewers and from editor Tim Elliott considerably improved this manuscript. This research was supported by a NERC urgency grant (NE/L000741/1).

Appendix A. Supplementary material

Supplementary material related to this article can be found online at http://dx.doi.org/10.1016/j.epsl.2015.03.025.

References

Alatorre-Ibarguengoitia, M.A., Scheu, B., Dingwell, D.B., 2011. Influence of the fragmentation process on the dynamics of Vulcanian eruptions: an experimental approach. Earth Planet. Sci. Lett. 302, 51–59.

Andronico, D., Cristaldi, A., Del Carlo, P., Taddeucci, J., 2009. Shifting styles of basaltic explosive activity during the 2002–03 eruption of Mt. Etna, Italy. J. Volcanol. Geotherm. Res. 180, 110–122.

Blundy, J., Cashman, K., 2001. Ascent-driven crystallisation of dacite magmas at Mount St Helens, 1980–1986. Contrib. Mineral. Petrol. 140, 631–650.

Blundy, J., Cashman, K., 2008. Petrologic reconstruction of magmatic system variables and processes. In: Putirka, K.D., Tepley, F.J. (Eds.), Minerals, Inclusions and Volcanic Processes, pp. 179–239.

Burgisser, A., Poussineau, S., Arbaret, L., Druitt, T.H., Giachetti, T., Bourdier, J.L., 2010. Pre-explosive conduit conditions of the 1997 Vulcanian explosions at Soufriere Hills Volcano, Montserrat: I. Pressure and vesicularity distributions. J. Volcanol. Geotherm. Res. 194, 27–41.

Carmichael, I.S.E., 2002. The andesite aqueduct: perspectives on the evolution of intermediate magmatism in west-central (105–99 degrees W) Mexico. Contrib. Mineral. Petrol. 143, 641–663.

Cashman, K., Blundy, J., 2000. Degassing and crystallization of ascending andesite and dacite. Philos. Trans. R. Soc. Lond. A, Math. Phys. Eng. Sci. 358, 1487–1513.

Cashman, K.V., 2004. Volatile controls on magma ascent and eruption. In: Sparks, R.S.J., Hawkesworth, C.J. (Eds.), State of the Planet: Frontiers and Challenges in Geophysics, pp. 109–124.

Clarke, A.B., Stephens, S., Teasdale, R., Sparks, R.S.J., Diller, K., 2007. Petrologic constraints on the decompression history of magma prior to Vulcanian explosions at the Soufriere Hills volcano, Montserrat. J. Volcanol. Geotherm. Res. 161, 261–274.

Cole, P.D., Calder, E.S., Sparks, R.S.J., Clarke, A.B., Druitt, T.H., Young, S.R., Norton, G.E., 2002. Deposits from dome-collapse and fountain-collapse pyroclastic flows at Soufrière Hills Volcano, Montserrat, from 1995 to 1999. In: Druitt, T.H., Kokelaar, B.P. (Eds.), The Eruption of Soufrière Hills Volcano. In: Geol. Soc. Lond. Mem., pp. 231–262.

Cole, P.D., Smith, P., Komorowski, J.C., Alfano, F., Bonadonna, C., Christopher, T., Loughlin, S.C., 2014. Precursory activity, ash venting and minor explosive activity at Soufriere Hills Volcano, Montserrat 2005 to 2010. In: Wadge, G., Robertson, R., Voight, B. (Eds.), The Eruption of Soufrière Hills Volcano, Montserrat from 2000 to 2010. Montserrat from 2005 to 2010. In: Mem. Geol. Soc., London.

Couch, S., Harford, C.L., Sparks, R.S.J., Carroll, M.R., 2003a. Experimental constraints on the conditions of formation of highly calcic plagioclase microlites at the Soufriere Hills Volcano, Montserrat. J. Petrol. 44, 1455–1475.

Couch, S., Sparks, R.S.J., Carroll, M.R., 2003b. The kinetics of degassing-induced crystallization at Soufriere Hills volcano, Montserrat. J. Petrol. 44, 1477–1502.

Dalton, M.P., Watson, I.M., Nadeau, P.A., Werner, C., Morrow, W., Shannon, J.M., 2009. Assessment of the UV camera sulfur dioxide retrieval for point source plumes. J. Volcanol. Geotherm. Res. 188, 358–366.

Edmonds, M., Herd, R.A., 2007. A volcanic degassing event at the explosive-effusive transition. Geophys. Res. Lett. 34, L21310. http://dx.doi.org/10.1029/2007GL031379.

Edmonds, M., Oppenheimer, C., Pyle, D.M., Herd, R.A., Thompson, G., 2003. SO_2 emissions from Soufriere Hills Volcano and their relationship to conduit permeability, hydrothermal interaction and degassing regime. J. Volcanol. Geotherm. Res. 124, 23–43.

Eichelberger, J.C., Carrigan, C.R., Westrich, H.R., Price, R.H., 1986. Non-explosive silicic volcanism. Nature 323, 598–602.

Fischer, T.P., Roggensack, K., Kyle, P.R., 2002. Open and almost shut case for explosive eruptions: Vent processes determined by SO_2 emission rates at Karymsky volcano, Kamchatka. Geology 30, 1059–1062.

Galle, B., Oppenheimer, C., Geyer, A., McGonigle, A.J.S., Edmonds, M., Horrocks, L., 2003. A miniaturised ultraviolet spectrometer for remote sensing of SO_2 fluxes: a new tool for volcano surveillance. J. Volcanol. Geotherm. Res. 119, 241–254.

Gerlach, T.M., McGee, K.A., 1994. Total sulfur dioxide emissions and pre-eruption vapor-saturated magma at Mount St. Helens, 1980–88. Geophys. Res. Lett. 21, 2833–2836.

Gonnermann, H.M., Manga, M., 2007. The fluid mechanics inside a volcano. Annu. Rev. Fluid Mech., 321–356.

Hammer, J.E., Cashman, K.V., Hoblitt, R.P., Newman, S., 1999. Degassing and microlite crystallization during pre-climactic events of the 1991 eruption of Mt, Pinatubo, Philippines. Bull. Volcanol. 60, 355–380.

Hirabayashi, J., Ohba, T., Nogami, K., Yoshida, M., 1995. Discharge rate of SO_2 from Unzen Volcano, Kyushu, Japan. Geophys. Res. Lett. 22, 1709–1712.

Holland, A.S.P., Watson, I.M., Phillips, J.C., Caricchi, L., Dalton, M.P., 2011. Degassing processes during lava dome growth: insights from Santiaguito lava dome, Guatemala. J. Volcanol. Geotherm. Res. 202, 153–166.

Kantzas, E.P., McGonigle, A.J.S., Tamburello, G., Aiuppa, A., Bryant, R.G., 2010. Protocols for UV camera volcanic SO_2 measurements. J. Volcanol. Geotherm. Res. 194, 55–60.

Kennedy, B., Spieler, O., Scheu, B., Kueppers, U., Taddeucci, J., Dingwell, D.B., 2005. Conduit implosion during Vulcanian eruptions. Geology 33, 581–584.

Kennedy, B.M., Jellinek, A.M., Russell, J.K., Nichols, A.R.L., Vigouroux, N., 2010. Time- and temperature-dependent conduit wall porosity: a key control on degassing and explosivity at Tarawera volcano, New Zealand. Earth Planet. Sci. Lett. 299, 126–137.

Kraus, S.G., 2006. DOASIS, A Framework Design for DOAS. University of Manheim.

Lane, S.J., Phillips, J.C., Ryan, G.A., 2008. Dome-building eruptions: insights from analogue experiments. In: Lane, S.J., Gilbert, J.S. (Eds.), Fluid Motions in Volcanic Conduits: A Source of Seismic and Acoustic Signals, pp. 207–237.

Lautze, N.C., Houghton, B.F., 2007. Linking variable explosion style and magma textures during 2002 at Stromboli volcano, Italy. Bull. Volcanol. 69, 445–460.

Lavallee, Y., Varley, N.R., Alatorre-Ibarguengoitia, M.A., Hess, K.U., Kueppers, U., Mueller, S., Richard, D., Scheu, B., Spieler, O., Dingwell, D.B., 2012. Magmatic architecture of dome-building eruptions at Volcán de Colima, Mexico. Bull. Volcanol. 74, 249–260.

Mangan, M., Mastin, L., Sisson, T., 2004. Gas evolution in eruptive conduits: combining insights from high temperature and pressure decompression experiments with steady-state flow modeling. J. Volcanol. Geotherm. Res. 129, 23–36.

Michaut, C., Ricard, Y., Bercovici, D., Sparks, R.S.J., 2013. Eruption cyclicity at silicic volcanoes potentially caused by magmatic gas waves. Nat. Geosci. 6, 856–860.

Miwa, T., Geshi, N., 2012. Decompression rate of magma at fragmentation: inference from broken crystals in pumice of vulcanian eruption. J. Volcanol. Geotherm. Res. 227, 76–84.

Miwa, T., Geshi, N., Shinohara, H., 2013. Temporal variation in volcanic ash texture during a vulcanian eruption at the Sakurajima volcano, Japan. J. Volcanol. Geotherm. Res. 260, 80–89.

Miwa, T., Toramaru, A., Iguchi, M., 2009. Correlations of volcanic ash texture with explosion earthquakes from vulcanian eruptions at Sakurajima volcano, Japan. J. Volcanol. Geotherm. Res. 184, 473–486.

Moore, G., Carmichael, I.S.E., 1998. The hydrous phase equilibria (to 3 kbar) of an andesite and basaltic andesite from western Mexico: constraints on water content and conditions of phenocryst growth. Contrib. Mineral. Petrol. 130, 304–319.

Mori, T., Shinohara, H., Kazahaya, K., Hirabayashi, J.-i., Matsushima, T., Mori, T., Ohwada, M., Odai, M., Iino, H., Miyashita, M., 2013. Time-averaged SO_2 fluxes of subduction-zone volcanoes: example of a 32-year exhaustive survey for Japanese volcanoes. J. Geophys. Res., Atmos. 118, 8662–8674.

Morrissey, M.M., Mastin, L.G., 2000. Vulcanian eruptions. In: Sigurddson, H. (Ed.), Encyclopedia of Volcanoes. Academic Press, pp. 463–476.

Nadeau, P.A., Palma, J.L., Waite, G.P., 2011. Linking volcanic tremor, degassing, and eruption dynamics via SO_2 imaging. Geophys. Res. Lett. 38, L01304. http://dx.doi.org/10.1029/2010GL045820.

Noguchi, S., Toramaru, A., Nakada, S., 2008. Relation between microlite textures and discharge rate during the 1991–1995 eruptions at Unzen, Japan. J. Volcanol. Geotherm. Res. 175, 141–155.

Platt, U., Stutz, J., 2008. Differential Optical Absorption Spectroscopy: Principles and Applications. Springer, pp. 1–4.

Platt, U.P., 1994. Differential optical absorption spectroscopy (DOAS). In: Sigrist, M.W. (Ed.), Air Monitoring by Spectroscopic Techniques. Wiley, New York.

Putirka, K.D., 2008. Thermometers and barometers for volcanic systems. In: Putirka, K.D., Tepley, F.J. (Eds.), Minerals, Inclusions and Volcanic Processes, pp. 61–120.

Reubi, O., Blundy, J., Varley, N.R., 2013. Volatiles contents, degassing and crystallisation of intermediate magmas at Volcán de Colima, Mexico, inferred from melt inclusions. Contrib. Mineral. Petrol. 165, 1087–1106.

Reubi, O., Sims, K.W.W., Varley, N.R., Reagan, M., Eikenberg, J., in press. Timescales of degassing and conduit dynamics inferred from ^{210}Pb–^{226}Ra disequilibria in Volcán de Colima 1998–2010 andesitic magmas. In: Chemical, Physical and Temporal Evolution of Magmatic Systems. Geol. Soc. Lond.

Rose, W.I., Luis Palma, J., Delgado Granados, H., Varley, N., 2013. Open-vent volcanism and related hazards: overview. In: Rose, W.I., Palma, J.L., Granados, H.D., Varley, N. (Eds.), Understanding Open-Vent Volcanism and Related Hazards, pp. VII–XIII.

Ruprecht, P., Worner, G., 2007. Variable regimes in magma systems documented in palgioclase zoning patterns: El Misti stratovolcano and Andahua monogenetic cones. J. Volcanol. Geotherm. Res. 165, 142–162.

Rutherford, M.J., Devine, J.D., 2003. Magmatic conditions and magma ascent as indicated by hornblende phase equilibria and reactions in the 1995–2002 Soufriere Hills magma. J. Petrol. 44, 1433–1454.

Rutherford, M.J., Hill, P.M., 1993. Magma ascent rates from amphibole breakdown: an experimental study applied to the 1980–1986 Mount St. Helens eruptions. J. Geophys. Res., Solid Earth 98, 19667–19685.

Salerno, G.G., Burton, M.R., Oppenheimer, C., Caltabiano, T., Randazzo, D., Bruno, N., Longo, V., 2009. Three-years of SO_2 flux measurements of Mt. Etna using an automated UV scanner array: comparison with conventional traverses and uncertainties in flux retrieval. J. Volcanol. Geotherm. Res. 183, 76–83.

Savov, I.P., Luhr, J.F., Navarro-Ochoa, C., 2008. Petrology and geochemistry of lava and ash erupted from Volcan Colima, Mexico, during 1998–2005. J. Volcanol. Geotherm. Res. 174, 241–256.

Scandone, R., Cashman, K.V., Malone, S.D., 2007. Magma supply, magma ascent and the style of volcanic eruptions. Earth Planet. Sci. Lett. 253, 513–529.

Scott, J.A.J., Mather, T.A., Pyle, D.M., Rose, W.I., Chigna, G., 2012. The magmatic plumbing system beneath Santiaguito Volcano, Guatemala. J. Volcanol. Geotherm. Res. 237, 54–68.

Self, S., Wilson, L., Nairn, I.A., 1979. Vulcanian eruption mechanisms. Nature 277, 440–443.

Sparks, R.S.J., Tait, S.R., Yanev, Y., 1999. Dense welding caused by volatile resorption. J. Geol. Soc. 156, 217–225.

Spieler, O., Kennedy, B., Kueppers, U., Dingwell, D.B., Scheu, B., Taddeucci, J., 2004. The fragmentation threshold of pyroclastic rocks. Earth Planet. Sci. Lett. 226, 139–148.

Stevenson, J.A., Varley, N., 2008. Fumarole monitoring with a handheld infrared camera: Volcán de Colima, Mexico, 2006–2007. J. Volcanol. Geotherm. Res. 177, 911–924.

Toramaru, A., Noguchi, S., Oyoshihara, S., Tsune, A., 2008. MND (microlite number density) water exsolution rate meter. J. Volcanol. Geotherm. Res. 175, 156–167.

Tuffen, H., Dingwell, D.B., Pinkerton, H., 2003. Repeated fracture and healing of silicic magma generate flow banding and earthquakes? Geology 31, 1089–1092.

Varley, N., Arambula-Mendoza, R., Reyes-Davila, G., Sanderson, R., Stevenson, J., 2010a. Generation of Vulcanian activity and long-period seismicity at Volcán de Colima, Mexico. J. Volcanol. Geotherm. Res. 198, 45–56.

Varley, N.R., Arambula-Mendoza, R., Reyes-Davila, G., Stevenson, J., Harwood, R., 2010b. Long-period seismicity during magma movement at Volcán de Colima. Bull. Volcanol. 72, 1093–1107.

Venezky, D.Y., Rutherford, M.J., 1999. Petrology and Fe–Ti oxide reequilibration of the 1991 Mount Unzen mixed magma. J. Volcanol. Geotherm. Res. 89, 213–230.

Vergniolle, S., Jaupart, C., 1986. Separated two-phase flow and basaltic eruptions. J. Geophys. Res., Solid Earth Planets 91, 2842–2860.

Walter, T.R., Legrand, D., Granados, H.D., Reyes, G., Arambula, R., 2013. Volcanic eruption monitoring by thermal image correlation: pixel offsets show episodic dome growth of the Colima volcano. J. Geophys. Res., Solid Earth 118, 1408–1419.

Webb, E.B., Varley, N.R., Pyle, D.M., Mather, T.A., 2014. Thermal imaging and analysis of short-lived Vulcanian explosions at Volcán de Colima, Mexico. J. Volcanol. Geotherm. Res., 278–279.

Williamson, B.J., Di Muro, A., Horwell, C.J., Spieler, O., Llewellin, E.W., 2010. Injection of vesicular magma into an andesitic dome at the effusive–explosive transition. Earth Planet. Sci. Lett. 295, 83–90.

Wright, H.M.N., Cashman, K.V., Mothes, P.A., Hall, M.L., Ruiz, A.G., Le Pennec, J.L., 2012. Estimating rates of decompression from textures of erupted ash particles produced by 1999–2006 eruptions of Tungurahua volcano, Ecuador. Geology 40, 619–622.

Wright, H.M.N., Cashman, K.V., Rosi, M., Cioni, R., 2007. Breadcrust bombs as indicators of Vulcanian eruption dynamics at Guagua Pichincha volcano, Ecuador. Bull. Volcanol. 69, 281–300.

Yokoo, A., Iguchi, M., Tameguri, T., Yamamoto, K., 2013. Processes prior to Outbursts of Vulcanian Eruption at Showa Crater of Sakurajima Volcano. Bull. Volcanol. Soc. Jpn. 58, 163–181.

Zobin, V.M., Luhr, J.F., Taran , Y.A., Breton, M., Cortes, A., De La Cruz-Reyna, S., Dominguez, T., Galindo, I., Gavilanes, J.C., Muniz, J.J., Navarro, C., Ramirez, J.J., Reyes, G.A., Ursua, M., Velasco, J., Alatorre, E., Santiago, H., 2002. Overview of the 1997–2000 activity of Volcán de Colima, Mexico. J. Volcanol. Geotherm. Res. 117, 1–19.